

RESEARCH ARTICLE

Optimal Network Reconfiguration and Scheduling With Hardware-in-the-Loop Validation for Improved Microgrid Resilience

YANG CHEN¹, (Member, IEEE), MOHAMMED OLAMA¹, (Senior Member, IEEE),
 MAXIMILIANO F. FERRARI², (Senior Member, IEEE),
 GUODONG LIU², (Senior Member, IEEE), QINGXIN SHI³, (Member, IEEE),
 ADITYA SUNDARARAJAN², (Senior Member, IEEE),
 BYUNGKWON PARK⁴, (Member, IEEE), ARTURO A. MASSOL-DEYA^{5,6}, (Member, IEEE),
 AND THOMAS B. OLLIS², (Senior Member, IEEE)

¹Computational Sciences and Engineering Division, Oak Ridge National Laboratory, Oak Ridge, TN 37831, USA

²Electrification and Energy Infrastructures Division, Oak Ridge National Laboratory, Oak Ridge, TN 37831, USA

³School of Electrical and Electronic Engineering, North China Electric Power University, Beijing 102206, China

⁴Department of Electrical Engineering, Soongsil University, Seoul 06978, South Korea

⁵Department of Biology, University of Puerto Rico at Mayagüez, Mayagüez, PR 00681, USA

⁶Casa Pueblo, Adjuntas, PR 00601, USA

Corresponding author: Mohammed Olama (olamahussem@ornl.gov)

This material is based upon work supported by the U.S. Department of Energy's Office of Energy Efficiency and Renewable Energy (EERE) under the Solar Energy Technologies Office Award Number DE-EE0002243-2144.

ABSTRACT With the increased occurrence of various major extreme weather events, power outages and prompt power system restorations have recently drawn more attention to the resilience and recovery of power systems. From the perspective of a more resilient power delivery at the distribution grid, system restoration using network topology reconfiguration together with optimal scheduling of distributed energy resources are adopted in this paper. The proposed optimization model aims at minimizing the total load shedding cost and other operational costs, in which linearized topological constraints borrowed from graph theory and linearized DistFlow models are respectively used to maintain the radial network topology and power flow balance after system contingencies. To demonstrate the applicability of the proposed strategy, a real-world case study of a networked three-microgrid system in Adjuntas, Puerto Rico, is used with the consideration of different independent/interconnected microgrid scenarios, contingencies, and fairness settings. Furthermore, hardware-in-the-loop testing is conducted for the same three-microgrid network, where the closely matched results with the simulated ones have validated the effectiveness of the proposed restoration strategy, which is now ready to move one step forward towards field deployment. Finally, to test the proposed restoration strategy in a larger networked system, the modified IEEE-33 bus test distribution system is considered, and the results show a more resilient power delivery for critical loads under three and four line outages.

INDEX TERMS Power grid resilience, system restoration strategy, networked microgrid, network topology reconfiguration, optimal asset scheduling, hardware-in-the-loop testing.

NOMENCLATURE

$\Delta p^L, \Delta q^L$ Real power, reactive load shedding at bus.

$\Delta p^V, z$ PV curtailment, binary line status.

η_V, η_c, η_d Efficiency of PV, battery charging, discharging.

γ, x, S Resistance, inductance, thermal limit of line.

$\bar{\alpha}_c, \bar{\alpha}_d$ Max coefficient of battery charging, discharging.

\bar{G}, \underline{G} Upper, lower limit of micro-turbine generation.

The associate editor coordinating the review of this manuscript and approving it for publication was Youngjin Kim¹.

\bar{U}, \bar{D}	Upper limit of ramping up, down.
\bar{V}, \underline{V}	Upper, lower limit of voltage.
$\pi(j), \delta(j)$	Set of parent, child buses of bus j .
ρ, ϵ	Degradation cost, loss cost of power flow.
$\alpha_b, \bar{\alpha}_b$	Min, max state-of-charge of battery.
C^G, C^L	Cost of micro-turbine and load shedding.
C^V, Sol	PV curtailment cost, solar radiation.
ec, ed	Charging, discharging power of battery.
ev, eb	Actual PV power usage, battery level.
$F_{i,j}, v$	Flow of branch ij in fictitious network, voltage at bus.
N, A, L	Set of total buses, islanded buses, lines.
N_G, N_V, N_B	Set of buses with generator, PV, battery.
P, IB	Real power load, initial battery energy level.
p^G, q^H	Power output of micro-turbine, shunt capacitor.
p^N, q^N	Real, reactive power injection at bus.
pf, qf	Real, reactive power flow of line.
Q, SH	Reactive power load, capacity of shunt capacitor.
SV, SB	Size of PV panel, energy capacity of battery.
$t, i/j$	Index of time, bus ($i \neq j$).

I. INTRODUCTION

A. BACKGROUND

Since the U.S. Energy Information Administration began collecting electricity reliability data in 2013, electricity customers in the U.S. experienced, on average, just over eight hours of electric power interruptions annually, while taking major events into account. When major events (hurricanes, snowstorms, wildfires, etc.) are excluded, the average interruption duration was around two hours consistently from 2013 to 2020 [1]. Different factors cause power interruptions, including extreme weather, vegetation patterns, utility practices, cyberattacks, etc. It is reported that about 83% of major outages in the U.S. between 2000 and 2021 were attributed to weather-related events, which are expected to intensify as the climate warms [2]. The average annual number of weather-related power outages increased by roughly 78% in the decade of 2011-2021 as compared to the decade of 2000-2010.

In recent years, the 2021 Dixie wildfire was caused by the blowing of two fuses when a tree (Douglas fir) fell on an electrical distribution line [3], which led to outages that affected around 20 counties in northern California. The rare winter storm Uri in 2021 impacted 25 states, in which Texas was hit the hardest [4]. At least 210 deaths were caused by the storm, and the related financial losses were over \$120 billion [5]. Due to the freezing temperatures, electricity generators began experiencing outages, and controlled blackouts occurred to reduce energy usage. Multiple factors caused those extended blackouts, including that the Electric Reliability Council of Texas (ERCOT) underestimated the peak demand by nearly 14%, and weather forecasts misjudged the severity and timing of the storm [6], [7]. Although not the most severe Texas

winter storm on record, Uri caused the most loss of electricity and narrowly missed a catastrophic failure that could cause a total blackout throughout the state [6].

On Sep. 6, 2017, hurricane Irma (Category 5) struck Puerto Rico and caused 1.1 million customers losing power. Only two weeks later, hurricane Maria (Category 4) made landfall in Puerto Rico, and satellite images showed 80% decrease in lighting immediately [8]. Maria has caused the longest blackout in the U.S. history. The increasing occurrence of various major events and their catastrophic power outage consequences have drawn more attention to the resilience and recovery of power systems. On Sep. 18, 2022, hurricane Fiona has made landfall in Puerto Rico [9], which triggered an island-wide blackout for nearly 1.5 million customers.

Although various definitions and metrics for reliability and resilience have been suggested in literature, the broadly agreed upon understanding is that reliability usually takes binary functional or failed view on the system [10], whereas resilience, which is derived from the Latin word, *resilio* [11] and means to “spring back”, commonly refers to the ability of a system to recover from disruptive events. Network system planning in power systems usually addresses enhancing the reliability of the system, where the objective is to maintain the supply of electricity under traditional contingencies such as the loss of generation, loss of transmission line, or a substation trips off. For example, from a practical operational perspective, the most widely used reliability protocol is the “normal minus one” (N-1) standard. A power system can be described as being N-1 secure when it is capable of maintaining normal operations in the event of a single contingency event, such as the unplanned loss of a transmission line, generator, or transformer.

On the other hand, resilience encompasses additional concepts - preparing for, operating through, and recovering from significant disruptions, no matter what the cause is. It is about the ability to withstand extreme or prolonged events. The main characteristics of reliability and resiliency can be distinguished from respectively the (high, low) probability and (low, high) impact of a disruptive event. Such an impact affects restoration time, outage duration, fault number, main objective of concerns, evaluation indices, etc. [11]. In extreme events, the operator probably won't be able to manually determine in a timely manner what switching lines (tie lines and sectionalizing lines) that need to be closed or opened together with optimizing the power generation of the available distributed energy resources (DERs) in the system, especially for a relatively large system. However, this can simply be performed using a comprehensive, optimized restoration strategy that can be implemented in real time to minimize the load shedding in the system.

B. RELATED WORKS AND LIMITATIONS

Associated with an extreme event, grid conditions can be categorized into four states: prevention, degradation, restoration, and adaptation states [12]. The grid functionality forms

a resilience triangle or trapezoid curve depending on whether restoration action is implemented promptly or not after the degradation state. Different approaches have been proposed to model and improve the restoration process and estimate the restoration time, e.g., statistical modeling [13], [14], agent-based simulations [15], and optimization approaches [16], [17]. Note that about 90% of all outages occur at the distribution system level [18].

From the perspective of preparedness and resilience enhancement for power distribution systems, several studies on pre-event planning and immediate post-event responsive operation have been introduced in literature and grouped into four categories: (1) hardening strategies on the power infrastructure [19], [20] [21], [22], (3) providing power to the affected areas using mobile generation resources as backups [23], [24] [25], [26], (4) reducing flexible loads using demand response programs [27], [28] [29], [30] [31], and (5) reconfiguring the topology of the distribution network and dynamic forming of microgrids (MGs) after outage events [32], [33] [34], [35] [36], [37] [38]. A brief review of these four proposed resilience solutions is presented next.

To strengthen power distribution systems against natural calamity, hardening strategies on the power infrastructure have been employed in accordance with need. “Infrastructure hardening should not come only as a result of storm damage and teardowns, but as part of a regular maintenance schedule” [19], [39]. Infrastructure hardening and condition-based maintenance scheduling are integrated together for critical components of the power systems by Markov decision processes, and the system survival functions against hurricanes are derived as a dynamic stress-strength model in the framework of [19]. Two hardening strategies have been modeled depending on the infrastructure type and its geographical location: with *temporary* effect (e.g., repeated vegetation trimming in a specific time period) and *permanent* effect (e.g., undergrounding of transmission lines, pole reinforcing, installation of spacer cables and cutout-mounted reclosers). A hybrid physics-based and data-informed Monte Carlo simulation model is presented in [20] to improve the prediction capability on power outages while capturing the parameters related to the power infrastructure. The proposed model is calibrated using historic power outage data, and pole replacement is used as demonstrative hardening case studies for the methodology. A tri-level defender-attacker-defender model is built in [21] to optimize the line hardening plan, where at the first level the defender makes hardening decision, the attacker makes the worst damage at the second level, and at the third level the system operator takes operational resilience strategies such as islanding formation and topology reconfiguration to reduce load shedding. The life-cycle resilience analysis of power distribution systems requires tracking the reliability of utility poles over time [22]. Thus, the long-term resilience maximization problem of a distribution system is formulated in [22] as a Markov decision process and solved using deep

reinforcement learning framework integrated with a novel risk-based ranking strategy. The obtained optimal hardening strategy is applied for a large power distribution system consisting of over 7,000 poles. Comparison results show that the cumulative expected resilience of a power distribution system can be improved by about 30% with respect to the U.S. National Electric Safety Code over 100 years period of planning horizon.

Another straightforward countermeasure to deal with potential disastrous threats in power distribution systems is to provide power by mobile generation resources. Mobility-as-a-service for resilience delivery in power distribution systems has been investigated in [23]. The developed optimization model coordinates the mobile power sources utilization with repair crew schedules in consideration of both energy and transportation networks. The results show potential in boosting resilience and operational endurance of mission-critical systems. To increase both the survivability and restoration capabilities of a distribution system, a two-stage stochastic mixed-integer model is constituted in the first stage to pre-position crews and mobile emergency generators to hasten post-event operations, which are simulated using scenario generation in the second stage [24]. Since manually changing the switches is a time-consuming action, finding the switching sequence considering crew team’s travel time is critical in the first stage operation. Energy storage systems (ESS) are validated as back-up resources during events, but they are often installed at locations with greatest economic value during normal operations [25]. In addition to stationary ESS, a two-stage stochastic second-order conic program is proposed in [25] to optimize the investment/installment of mobile ESS units in the first stage and re-route these storage units to form dynamic MGs in the second stage for the purpose of reducing load shedding. A progressive hedging algorithm is applied for solving the model. A novel idea of separable mobile ESS (vehicle carrier and storage modules) is proposed in [40], hence, the vehicle carrier, storage module, mobile emergency generators, and fuel tankers (to feed generators) are jointly routed and scheduled throughout the distribution system. Being an essential mobile storage, an on-call electric vehicle fleet is integrated in a resiliency-driven multi-step restoration strategy in [26] for a seismic event. The random characteristic of the event is generated by Monte Carlo simulation, and the stochasticity of electric vehicle mobility (number and location) in the related zone is forecast by learning-based analysis (Prophet Algorithm developed by Facebook). Numerical results have shown that the load restoration is increased within a range of 71%-95% depending on event duration/location, available electric vehicles, and socket number.

Another operational strategy for improving resilience is to reduce the flexible load by demand response programs, which can reveal and utilize the demand flexibility by enabling the participation of a large number of grid-interactive efficient buildings (GEB). To leverage the flexibility of demand

response in a distribution service restoration, a three-step framework is proposed in [27] by modeling three optimization problems to 1) determine the feasible controllable aggregated load for each bus in the network, 2) determine buses to perform demand response with the load target, and 3) maintain load target in each household via home energy management. A case study on the IEEE 123 bus test system showed improvement in resilience in terms of energy restored. The work in [30] introduced a scalable hierarchical transactional control strategy, where a Stackelberg game in the upper layer and a model-free controller in the lower layer are used to optimally schedule GEB loads (e.g., HVAC units and water heaters) to support grid services. The effectiveness of the proposed transactional control strategy was demonstrated through a large-scale case study including 10,000 GEB, and the results showed improved system resiliency. A data-driven, distributed version of the same hierarchical transactional control strategy, which leverages concepts from machine learning, game theory, and model-free control, was proposed in [31].

Besides infrastructure hardening, additional mobile backup generation, and demand response, another main research stream has focused on boosting resilience of distribution systems by network topology reconfiguration and dynamic MG formation under outage events. A soft open point is an emerging power electronic device to realize such reconfiguration by connecting feeders or networked MGs [32]. After line faults, the reconfiguration is implemented by switching tie lines and sectionalizing lines [33] while maintaining radial network topology to minimize load shedding and accumulative operation cost. This topology reconfiguration based outage management strategy outperforms MG formation approaches [34] when the distribution system has several normally-open tie lines and low penetration of DERs. A multi-step probabilistic model is designed to simulate the storm impact based on the geographic information of the distribution grid and the strength of its components (e.g., poles). Then, the optimal placement of switches along with distributed generation units are studied from the perspective of resilience of distribution systems [35]. To expand the coverage of distributed generation units, the MG formation problem is optimized in real-time operation by controlling the automatic switches and generation output to maximize the total served critical loads while satisfying self-adequacy, topological and operational constraints [36]. Furthermore, an adaptable directed multi-commodity flow-based microgrid formation model is utilized in [41] to restore the integrated electricity and gas network after an event landfall, considering distributed generators, power-to-gas facilities, and the rescheduling of generation units as operational resources.

The communication challenge under natural disasters has also been coped with by designing a distributed multi-agent coordination scheme via local communications. A methodological framework to dynamically change the boundaries of

MGs is developed in [37] by determining the operating modes of distributed generators and the on-off statuses of smart switches to aid fault isolation and load restoration. The proposed framework is thoroughly investigated with respect to feedback control of synchronous generators, maintaining frequency and voltage levels. A systematic method is presented in [42] to segment parts of the power distribution system into several microgrids with flexible boundaries, allowing them to merge and reconfigure dynamically to ensure maximum supply to critical loads. The deep reinforcement learning method in [38] is designed for topology transformable MGs, where the online dynamic multi-microgrid formation problem is formulated as a Markov decision process. Since the essence of the reconfiguration is to find all spanning forests, the solution space is exponentially increasing due to the flexible switching operations. Hence, a topology transformation method and action-decoupling Q-value are applied to satisfy radial topology requirement and reduce the possible action space efficiently. A holistic optimal topology design framework is proposed in [43], comprising six stages: generating network topologies, optimizing asset placement, assessing stability, analyzing post-outage flows, quantifying resilience metrics, and ranking topologies. This approach aims to address gaps in microgrid topology planning by ensuring both stability and resilience through a detailed evaluation of various topologies.

Lastly, a limited number of works presented hardware prototype/field testing and validation of the various restoration strategies in more realistic environments. The known demonstrations that practically validate coordination and control methods for individual MGs include 1) the Smart Power Infrastructure Demonstration for Energy Reliability and Security (SPIDERS) programs [44], which aim to provide highly reliable and resilient power to military bases; 2) the Portland Gas and Electric project [45] in Salem, Oregon, which is part of the Pacific Northwest Smart Grid Demonstration Project; 3) the Santa Rita jail project [46], which allows the jail to disconnect from the grid seamlessly and quickly and run islanded for extended periods; 4) the University of California, Irvine (UCI) campus MG [47], which aims at testing how MGs operate internally as well as how they interface with the rest of the future smart grid; 5) the Borrego Springs MG [48], which serves a community of 2800 customers and exemplifies an “unbundled utility MG,” where distribution assets are owned by the utility, but the DERs are owned by independent power producers and customers; and 6) the Illinois Institute of Technology MG [49], which was designed and built to be the world’s first self-healing and efficient smart MG distribution system with enhanced reliability, new sustainable energy sources, and smart building automation technologies.

As a result, sizable research has been conducted on resilience enhancement of power distribution systems and MGs from different aspects in seeking power infrastructure modernization, event impact mitigation, and quick

post-event recovery. However, existing literature misses three crucial points: (1) Almost all existing literature focuses on system modeling and algorithm development with *simulation-only testing and validation*. Only few works present hardware prototype/field testing and validation of the various coordination and control strategies in realistic environments. Furthermore, these limited number of works have not explicitly addressed the resiliency aspect of distribution/microgrid systems. (2) Most of the proposed models and optimization restoration strategies are complex and computationally expensive, requiring large computational resources and thus *cannot be implemented in real-time*. (3) Most of the proposed models and optimization restoration strategies are *not comprehensive*, i.e., they do not consider all the various power system aspects together such as topology reconfiguration, power flow, line and voltage limits, as well as the various DERs, such as photovoltaic (PV) generation, ESS, micro-turbines (MTs), and demand response.

C. PROPOSED WORK AND MAIN CONTRIBUTIONS

Motivated by the aforementioned limitations, this study bridges such gaps by introducing a *real-world* case study and a *hardware-in-the-loop (HIL)* testing and validation for the proposed *comprehensive* optimal network reconfiguration and asset scheduling restoration strategy to improve distribution systems and MGs resilience during extreme events such as hurricanes. The proposed strategy makes use of the available switches and different types of dispatchable and non-dispatchable DERs. It is comprehensive by considering network topology reconfiguration, power flow, PV generation, ESS, MTs, shunt capacitors, and demand response. Linear topological constraints borrowed from the graph theory literature are used to ensure radial network topology after contingencies, perhaps in multiple islands. Several simulations and HIL testing case studies are conducted for a real-world 3-MG network located in Adjuntas, Puerto Rico to verify the effectiveness of the proposed restoration strategy. HIL testing allows for real-time verification and accounts for the nonlinear system dynamics and communication delays that are typically ignored in offline simulation-only environments.

In a nutshell, the main contributions of the research presented in this paper are highlighted as follows:

- 1) The proposed restoration strategy is tested using *HIL test platform* and real data collected from a *real-world* 3-MG network system in Adjuntas, Puerto Rico to demonstrate its effectiveness and move the current theoretical optimization one step towards actual field deployment. The testing considers several scenarios under different contingencies, independent/connected MGs conditions, daily/weekly runs, battery operation fairness, etc. The restoration strategy is further tested on a larger system using the modified IEEE 33-bus distribution network.

- 2) A *comprehensive* network reconfiguration and asset scheduling restoration strategy is developed that is fully linear and thus can easily be implemented in *real time*.

D. PAPER ORGANIZATION

The organization of this research is as follows. In Section II, the mathematical model for the proposed comprehensive optimal network reconfiguration and DER scheduling restoration strategy is derived. In Section III, the effectiveness of the proposed restoration strategy is demonstrated using HIL testing on the real-world 3-MG system in Puerto Rico. In Section IV, the modified IEEE 33-bus distribution system is used to further validate the proposed restoration strategy on a larger network. Finally, the conclusions are drawn in Section V.

II. MATHEMATICAL MODELING OF THE PROPOSED RESTORATION STRATEGY

In this section, the proposed optimal network reconfiguration and asset scheduling restoration strategy is presented. The optimization objective function together with the operational constraints for distribution systems/networked MGs are developed, including the constraints for the network topology as well as the operational constraints for the available DERs, such as MTs, solar PV panels, battery ESS, and line power flows.

- (1) Objective function

$$\begin{aligned} \min C_{sys} &= \sum_{i,t} [C^G \cdot p_{i,t}^G + C_i^L \cdot \Delta p_{i,t}^L \\ &+ C_i^V \cdot \Delta p_{i,t}^V + \rho \cdot (ec_{i,t} + ed_{i,t})] + \sum_{ij,t} \epsilon \cdot pf_{ij,t}^2 \end{aligned} \quad (1)$$

The objective function of the proposed operation model is to minimize the total system cost, which consists of the total MT generation cost, the total load shedding cost, the total PV curtailment cost, the total battery degradation cost, and the total power line loss cost. Here, for the sake of conciseness, the total power line loss cost is simplified to be dependent on the quadratic real power flow in the last term of Eq.(1). This quadratic term can be approximated by an absolute value term and then linearized, or it can directly be piecewise linearized.

- (2) Network topology & line switching constraints

$$\sum_{ij} z_{ij} = |N| - 1 - |A|, \forall ij \in L \quad (2)$$

$$\sum_{k \in \delta(j)} F_{jk} - \sum_{i \in \pi(j)} F_{ij} = -1, \forall j \in (N - S), j \neq 1 \quad (3)$$

$$\sum_{k \in \delta(j)} F_{jk} - \sum_{i \in \pi(j)} F_{ij} = 0, \forall j \in A \quad (4)$$

$$\sum_{k \in \delta(j)} F_{jk} = |N| - 1 - |A|, j = 1 \quad (5)$$

$$-M_1 \cdot z_{ij} \leq F_{ij} \leq M_1 \cdot z_{ij}, \forall ij \in L \quad (6)$$

When line faults occur, the center controller wants to reconfigure the network to a new radial topology that minimizes the required load shedding considering the line thermal limits, bus voltage limits, and other physical constraints of DERs. Normally, the distribution power grid has “radial structure”, which is also defined as a tree (connected graph without cycles) in a directed graph. In order to represent the

network topology, a lossless fictitious network is introduced here, similar to [33] and [50], where each non-source bus is assumed to have the unity load demand 1.0, as shown in Figure 1. Eqs.(2)-(6) are used to define such radial topology based on graph theory.

Eq.(2) defines the total number of closed lines as the total number of non-source buses minus the islanded buses, where $|\cdot|$ represents the dimension of a vector. An islanded bus means that it cannot be reached from a source bus. For example, if lines (4,5) and (5,6) in the fictitious network in Figure 1 are tripped, then bus 5 cannot be connected to the source bus via the tie line (6,9). In this case, the set $A = \{5\}$. If only one line (4,5) is tripped, then $A = \phi$. For a source bus, Eq.(5) defines its total line flow number as the total number of non-source buses minus the islanded buses. For non-source buses and islanded buses, the line flow balance is respectively defined in Eq.(3) and Eq.(4). z_{ij} is a binary variable to indicate whether the line switch is closed or not. M_1 is a sufficiently large number, it can be set as a number that is slightly larger than the estimated maximum of F_{ij} .

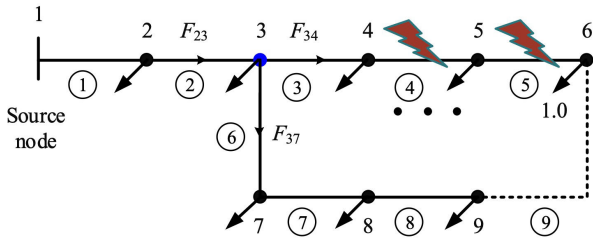


FIGURE 1. Example of a partially connected network under a two-line fault.

(3) MT & PV generation constraints

$$\underline{G} \leq p_{i,t}^G \leq \bar{G}, \forall i \in N_G \quad (7)$$

$$p_{i,t}^G - p_{i,t-1}^G \leq \bar{U}, \forall i \in N_G \quad (8)$$

$$p_{i,t-1}^G - p_{i,t}^G \leq \bar{D}, \forall i \in N_G \quad (9)$$

$$ev_{i,t} + \Delta p_{i,t}^V = SV \cdot Sol \cdot \eta_V, \forall i \in N_V \quad (10)$$

For a bus with a MT, Eq.(7) constraints turbine power output within its operational range, and Eqs.(8)-(9) restrict its ramp up and ramp down limit in each time step. Total solar PV power generation and its actual usage (or curtailment) can be estimated using Eq.(10). For more accurate PV generation, we refer readers to [51], which considers the PV panel angle, temperature, etc.

(4) Battery charging/discharging constraints

$$0 \leq ec_{i,t} \leq SB_i \cdot \bar{\alpha}_c, \forall i \in N_B, t \quad (11)$$

$$0 \leq ed_{i,t} \leq SB_i \cdot \bar{\alpha}_d, \forall i \in N_B, t \quad (12)$$

$$SB_i \cdot \underline{\alpha}_b \leq eb_{i,t} \leq SB_i \cdot \bar{\alpha}_b, \forall i \in N_B, t \quad (13)$$

$$eb_{i,1} = IB_i + (ec_{i,1} - ed_{i,1}) \cdot \Delta t, \forall i \in N_B \quad (14)$$

$$eb_{i,t} - eb_{i,t-1} = (ec_{i,t} - ed_{i,t}) \cdot \Delta t, \forall i \in N_B, t \quad (15)$$

Battery operation is modeled by the group of constraints Eqs.(11)-(15) [28], [29]. Specifically, charging/discharging energy of a battery in each time step is limited by its energy capacity and corresponding maximum charging/discharging coefficients in Eqs.(11)-(12). Stored energy level should always be within the allowable range determined by its energy capacity and min/max state-of-charge (SOC) coefficient in Eq.(13). Eqs.(14)-(15) are the energy balance based on charging/discharging activities. Δt is the hour length of each time step, e.g., 1 hour, 1/4 hour (15 minutes), etc.

(5) Nodal power and flow balance constraints

$$p_{i,t}^N = p_{i,t}^G + ev_{i,t} + (edi_{i,t} \cdot \eta_d - ec_{i,t} / \eta_c) - (P_{i,t} - \Delta p_{i,t}^L), \forall i \in N, t \quad (16)$$

$$q_{i,t}^N = q_{i,t}^H - (Q_{i,t} - \Delta q_{i,t}^L), \forall i \in N, t \quad (17)$$

$$\frac{P_{i,t}}{Q_{i,t}} \cdot \Delta q_{i,t}^L = \Delta p_{i,t}^L \leq P_{i,t}, \forall i \in N, t \quad (18)$$

$$q_{i,t}^H = SH \cdot v_{i,t}^2 \approx SH \cdot (2 \cdot v_{i,t} - 1), \forall i \in N, t \quad (19)$$

$$P_{j,t}^N = \sum_{k \in \delta(j)} pf_{jk,t} - \sum_{i \in \pi(j)} pf_{ij,t}, \forall j \in N, j \neq 1 \quad (20)$$

$$q_{j,t}^N = \sum_{k \in \delta(j)} qf_{jk,t} - \sum_{i \in \pi(j)} qf_{ij,t}, \forall j \in N, j \neq 1 \quad (21)$$

$$-M_2 \cdot z_{ij} \leq pf_{ij,t} \leq M_2 \cdot z_{ij}, \forall ij \in L \quad (22)$$

$$-M_2 \cdot z_{ij} \leq qf_{ij,t} \leq M_2 \cdot z_{ij}, \forall ij \in L \quad (23)$$

In this group of constraints, Eqs.(16)-(17) define the nodal real and reactive power injection balance, and Eqs.(20)-(21) provide real and reactive power flow balance based on the linearized DistFlow method [33]. In Eq.(16), power generation includes MT power generation, solar PV power generation, and discharging power from the battery, while power consumption consists of battery charging power and power demand. Reactive power generation is mainly provided here by shunt capacitors in Eq.(17). Eq.(18) expresses the assumed relationship between the real and reactive power of a load based on the power factor σ estimated from historical load profiles ($\frac{P_{i,t}}{Q_{i,t}} = \frac{\sigma_i}{\sqrt{1-\sigma_i^2}}$). The reactive power provided by shunt capacitors is proportional to voltage squared, which can be linearized by Eq.(19), since the bus voltage has a tight range. Eqs.(22)-(23) further assert that there will not be power flow through line (i, j) when the line is open.

(6) Voltage and line thermal constraints

$$\underline{V} \leq v_{i,t} \leq \bar{V}, \forall i \in N \quad (24)$$

$$-M_2 \cdot (1 - z_{ij}) \leq v_{i,t} - v_{j,t} - (r_{ij} \cdot pf_{ij,t} + x_{ij} \cdot qf_{ij,t}) / V_0, \forall ij \in L \quad (25)$$

$$v_{i,t} - v_{j,t} - (r_{ij} \cdot pf_{ij,t} + x_{ij} \cdot qf_{ij,t}) / V_0 \leq M_3 \cdot (1 - z_{ij}), \forall ij \in L \quad (26)$$

$$-2 \cdot S_{ij} \leq \sqrt{3} \cdot pf_{ij,t} + qf_{ij,t} \leq 2 \cdot S_{ij}, \forall ij \in L \quad (27)$$

$$-2 \cdot S_{ij} \leq \sqrt{3} \cdot pf_{ij,t} - qf_{ij,t} \leq 2 \cdot S_{ij}, \forall ij \in L \quad (28)$$

$$-S_{ij} \leq pf_{ij,t} \leq S_{ij}, \forall ij \in L \quad (29)$$

The voltage upper and lower limits in Eq.(24) apply to all buses except the slack bus (substation bus). The voltage drop along the power line is defined in Eqs.(25)-(26), where V_0 is the rated voltage and usually set to be 1. If the line is closed ($z_{ij} = 1$), the voltage drop can be calculated by the line power flow and its resistance/inductance, otherwise, the voltage drop is unbounded. Similarly, M_2 and M_3 are sufficient large numbers. Eqs.(27)-(29) are the piecewise linear version for line thermal limits of distribution lines ($pf^2 + qf^2 = S^2$) [33].

The formulated optimization problem in (1)-(29) is a mixed-integer linear programming (MILP) model, which can easily be solved using any MILP solving method such as the standard branch-and-bound method [52]. In this paper, the commercial solver Gurobi [53] is used for solving the formulated MILP optimization model. It is highly efficient in solving MILP models. Note that the average solving time for a daily run of any use case in the 3-MG system is about 1.12 seconds. While the average solving time for a daily run for any cases in the IEEE 33-bus test system is about 1.93 seconds. This shows that the formulated model can easily be solved in a short period of time.

III. REAL-WORLD CASE STUDY & HIL TESTING OF THE PROPOSED RESTORATION STRATEGY ON THE ADJUNTAS 3-MG SYSTEM IN PUERTO RICO

In this section, a real-world case study for a 3-MG network located in Adjuntas, Puerto Rico is presented to test and validate the proposed network reconfiguration and asset scheduling outage management strategy using HIL testing. Adjuntas is a small mountainside municipality in Puerto Rico. Like many other rural areas in Puerto Rico, this small town was severely impacted by the events of hurricane Maria in 2017 and the subsequent long-term energy outages caused by the unreliable power system of the island. In response to the devastation experienced by the community, a community networked MG is being constructed to power local businesses in the town square that will serve as a resiliency center in the event of future natural disasters. This community-owned MG consists of three parallel MGs on a single feeder that uses PV panels along with battery ESS to provide electricity to the community. It is designed to benefit the community in two ways: During normal conditions, it will reduce the electricity costs for the businesses located in the town square. While during extreme event conditions, the MG becomes a resiliency center by providing power to the businesses in order to serve the affected community.

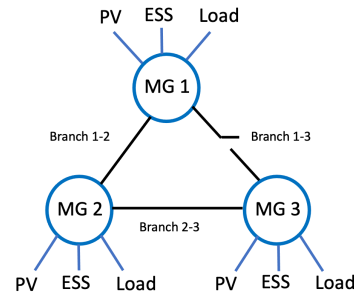
A. EXPERIMENTAL SETTING AND NUMERICAL RESULTS

Based on the actual MG system deployment in Plaza Public Adjuntas, Puerto Rico [54], three MGs are identified in Figure 2a. The overall MG system serves 14 businesses and 2 apartments, and it has various service entrance voltages as well as various service amperages. Figure 2b shows

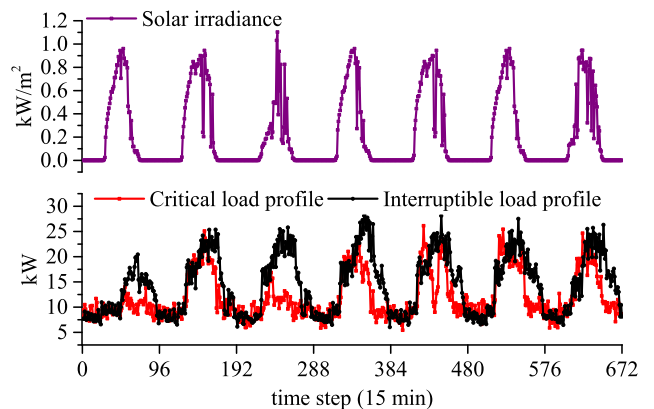
the single line diagram for the networked 3-MG system, which is designed to operate in islanded mode (disconnected from the main grid) under normal conditions. Under normal operation, MG1 is connected to MG2 which is connected to MG3, and thus the branch 1-3 is normally open. Each MG includes PV generation, ESS, and a load. For instance, MG2 supports six businesses, and it has single-phase PV inverters (SE5000H-US, SE7600H-US) as well as three-phase PV inverters (SE33KUS 480V/3-ph) to provide a total of 76 kW DC power. In addition, its ESS provides 663 kWh ($2 \times 221.4 \text{ kWh} + 2 \times 110 \text{ kWh}$) with inverter $2 \times$ Dynapower 125 kVA.



(a) Three MGs in Plaza Public Adjuntas.



(b) Single line diagram for the 3-MG network in Adjuntas.



(c) Measured solar irradiance and load profiles.

FIGURE 2. (a) Geospatial location of the studied 3-MG network, (b) its single line diagram, and (c) load & solar profiles. Note that (a) is a 3D render and the real system may differ, and the profiles in (c) were measured in 2019.

For the case study, the three MGs have solar PV power generation as the sole generation source and batteries as

TABLE 1. Basic parameters for the 3-MG system in adjuntas, puerto rico.

Microgrid	Rated PV power (kW)	Battery capacity (kWh)	Critical load	Voltage range (p.u.)	Total demand (kVA)
1	98.72	442	Yes	0.95-1.05	8096.61
2	76	663	No	0.95-1.05	9623.88
3	76	663	Yes	0.95-1.05	8096.61
Branch	Resistance (p.u.)	Inductance (p.u.)	Thermal limit (kVA)	—	—
1-2	0.3744	0.1238	100	—	—
2-3	0.3744	0.1238	100	—	—
1-3	0.3744	0.1238	100	—	—

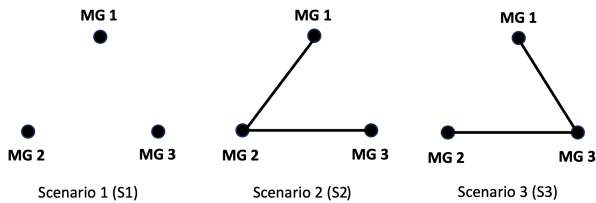


FIGURE 3. Single line diagrams of the three MGs in Adjuntas for the three scenarios (S1-S3) after reconfiguration.

ESS. Figure 2c shows one week (15 minute time resolution) solar irradiance and aggregated load profiles that are used in the case study. In this study, it is assumed that MG1 & MG3 support only critical loads (plotted in Figure 2c), while MG2 supports only interruptible loads (plotted in Figure 2c). Note that the critical and interruptible load profiles shown in Figure 2c are real aggregate load profiles collected from the test site. Other detailed energy system parameters are presented in Table 1. Note that there are three switches to connect the three MGs as a network. Other parameters for this 3-MG system operation are set as: the critical and interruptible load shedding costs are respectively $C^L = 1.5\$/kW$ and $0.4\$/kW$, the PV power curtailment cost is $C^V = 0.1\$/kW$, the battery degradation cost is $\rho = 0.008\$/kW$, the loss cost of power flow is $\epsilon = 0.01\$/kW$, the voltage range is set between 0.92-1.05 p.u., the charging and discharging efficiencies of the batteries are $\eta_c = \eta_d = 0.95$, $\bar{\alpha}_b = \bar{\alpha}_c = \bar{\alpha}_d = 1$, and $\underline{\alpha}_b = 0$. The proposed restoration strategy optimally selects the statuses of the three switches connecting the three MGs together with the optimal scheduling of the available DERs at each MG including PV generation, ESS, and loads, with the objective of minimizing load shedding and other system costs (PV curtailment cost and battery degradation cost).

In order to test the proposed restoration strategy under various and comprehensive conditions, several groups of different settings are designed and combined together to include all possible conditions. Note that for all the experiments herein, the SOC for each battery storage is not allowed to be lower than 20% at all times for emergency considerations.

Different scenario settings:

- Scenario 1 (S1): Independent scenario. The three MGs are disconnected, and thus each MG operates

independently without sharing power with the other MGs.

- Scenario 2 (S2): Connected scenario. The three MGs are connected, and thus they share power among themselves.
- Scenario 3 (S3): Connected scenario with line outage in branch 1-2. This scenario is similar to S2 but with one line outage.

Different run settings:

- Run 1 (R1): Weekly run. One week ahead optimization at one shot with 1-hour time step.
- Run 2 (R2): Daily run. One day ahead optimization with 15-minute time step. The restoration strategy runs once a day for one week with daily updates on the SOCs for all batteries.

Different contingency settings:

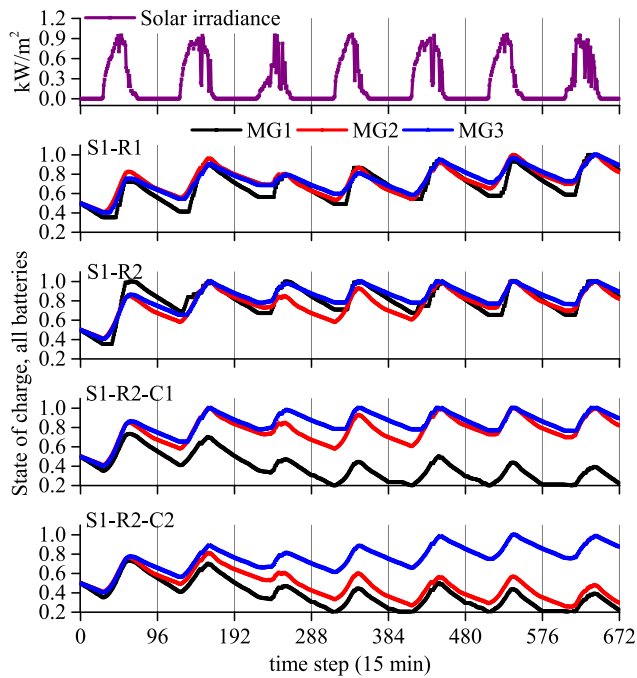
- ▶ Contingency 1 (C1): The generated PV power in MG 1 is reduced by 50% due to extreme weather.
- ▶ Contingency 2 (C2): The generated PV power in MG 1 is reduced by 50%, and the generated PV powers in MG2 and MG3 are both reduced by 15%.

Note that, in the realistic Adjuntas MG systems considered herein, the three MGs are in close vicinity. However, in general for other MG networks, they can be farther apart. Therefore, we considered two contingency settings to account for all possible cases. In Contingency 1, it is assumed that the extreme weather event has a hard hit on one of the MGs (assuming they are farther apart). While in Contingency 2, it is assumed that the extreme weather event affects all three MGs with different impact levels (assuming they are in close vicinity).

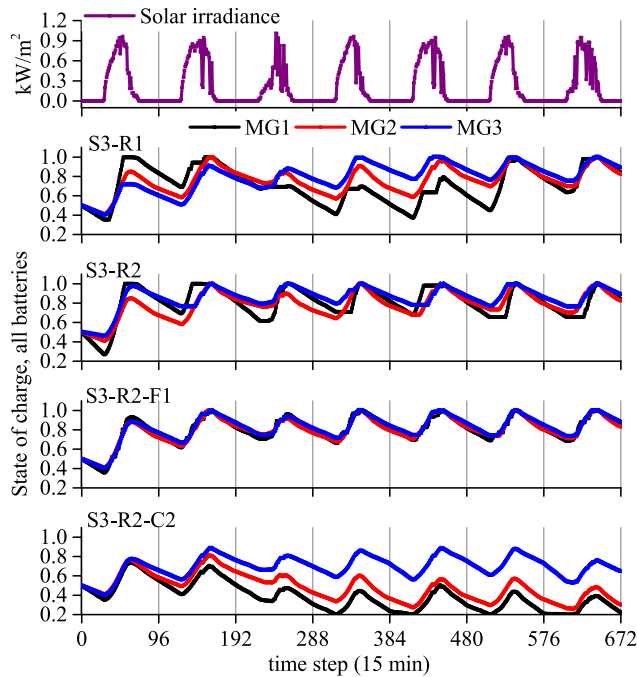
Different fairness settings:

- ◆ Fairness 1 (F1): The difference among the SOCs of all batteries in the three MGs should not exceed 5%. This setting prevents one or more batteries from running out faster than other batteries in the 3-MG system.

The single line diagrams for the three scenarios (S1-S3) of the 3-MG system after reconfiguration are illustrated in Figure 3, where the scheduling results for the SOCs of the three batteries are compared in Figure 4, and the corresponding PV generation curtailments are shown in Figure 5. The independent scenario (S1) is shown in Figure 4a, where each MG optimizes its own operation individually without any power exchange with the other MGs. Table 2 presents the numerical results for 14 different



(a) Battery SOCs for Scenario 1.

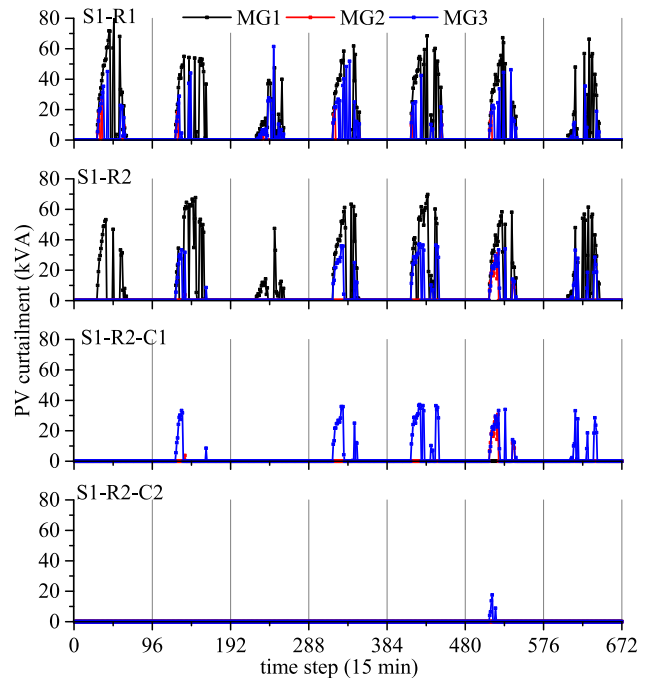


(b) Battery SOCs for Scenario 3.

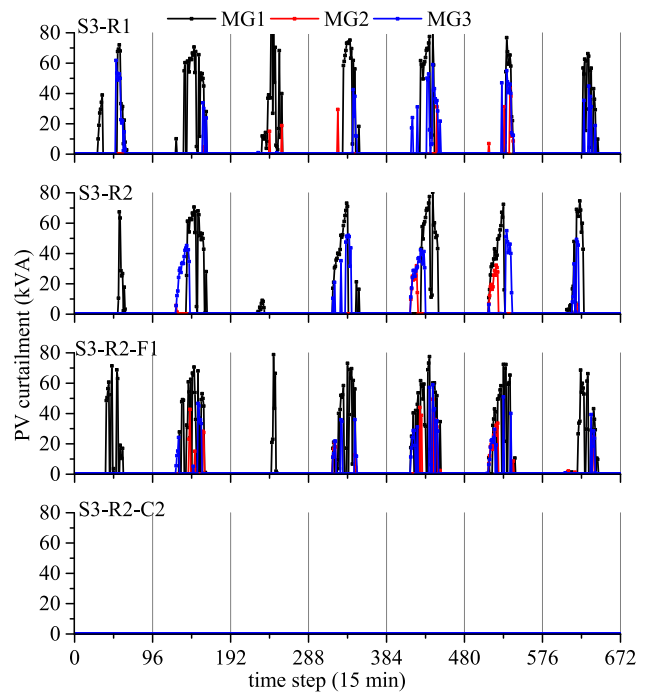
FIGURE 4. Battery SOCs for the three MGs in Puerto Rico under different settings.

combinations of independent/interconnected microgrid scenarios, contingencies, daily/weekly runs, and fairness settings.

For the different run settings S1-R1 and S1-R2, the SOC patterns for each MG are slightly different, but the detailed results in Table 2 have confirmed that the various results



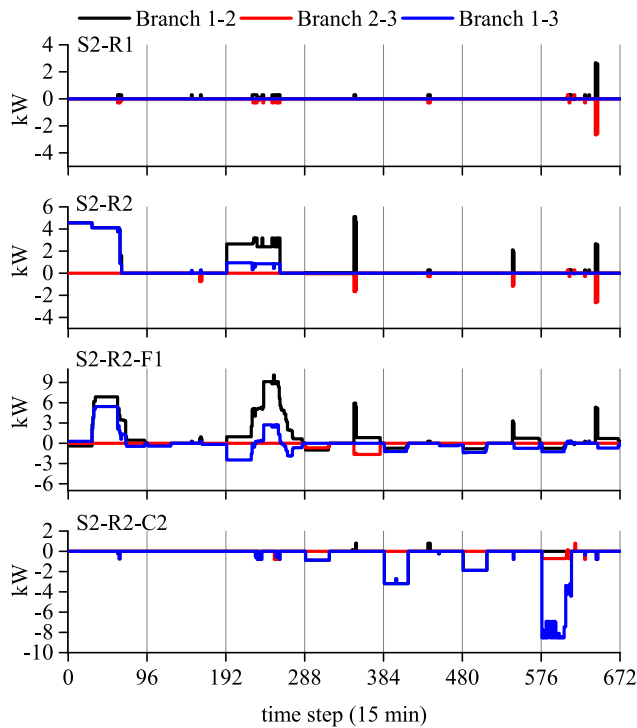
(a) PV curtailment for Scenario 1.



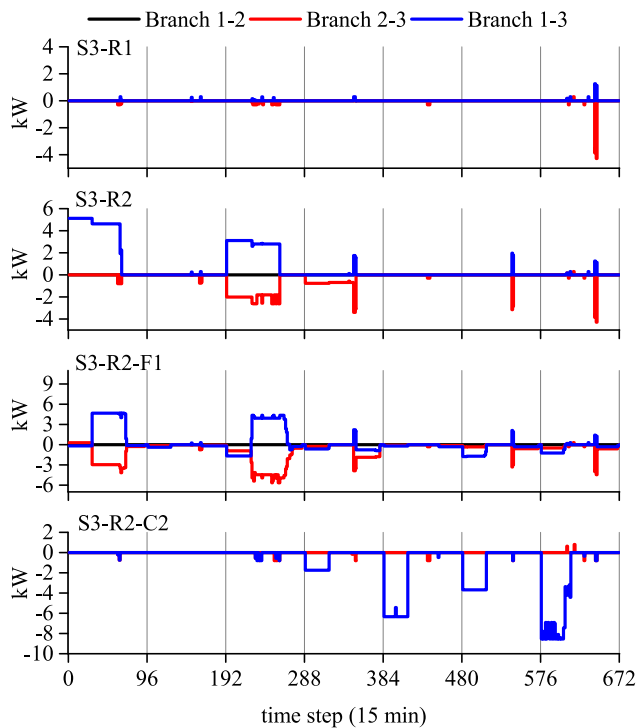
(b) PV curtailment for Scenario 3.

FIGURE 5. PV curtailment for the three MGs in Puerto Rico under different settings.

(e.g., PV curtailment, difference between total charging power and total discharging power) of the two run settings are the same. This is mainly because 1) the cost parameters in the model are fixed, 2) there is no power exchange among the three MGs under such scenario, and 3) there is sufficient solar PV power generation. With the consideration



(a) Branch power flows in Scenario 2.



(b) Branch power flows in Scenario 3.

FIGURE 6. Branch power flows among the three MGs in Puerto Rico under different settings.

of contingencies, we put our focus on the daily run (R2) for results demonstration because the weekly run (R1) is not that practical and its time resolution under contingency is

too low. With Contingency 1 setting in S1-R2-C1, the largest power generation source (MG1) has been reduced to half, therefore the SOC curve for MG1 battery started to approach 20% limit on the fourth day in Figure 4 due to its additional discharging operation to supply the demand. Also, note that the SOC for MG2 and MG3 batteries are the same as in S1-R2. Overall, for S1-R2-C1 in Table 2, the load of MG1 is shed 608.78 kW, and the overall discharged amount of MG1 battery is about 492.62 kW (total discharging minus total charging). For Contingency 2 setting in S1-R2-C2, the solar PV powers of both MG2 and MG3 are reduced 15% in addition to C1. Due to that, the SOC of MG2 is also leveled down slowly under this case, and the overall charged power amount of MG2 battery has flipped from 851.26 kW (in S1-R2-C1) to -536.36 kW (discharged). In contrast, the SOC of MG3 kept similar pattern as in S1-R2-C1. This is mainly because that MG3 supplies only critical load as shown in Table 1, and its total load is less than that of MG2 as shown in Figure 2c. Hence, under the same reduced rated PV and battery capacity, MG3 still has abundant solar power (50.53 kW curtailment) as shown in Table 2, and 992.77 kW is charged into its battery storage overall.

Now, with the connected scenarios S2 & S3, power can be shared among the three MGs. The power flow on the branches under different cases with S2 & S3 are plotted in Figure 6, where positive/negative power represents the power flow direction in the branch. In scenario S3, it is assumed that branch 1-2 has an outage, thus the three MGs are connected by the reconfigured topology branch 2-3 & branch 1-3 (see Figure 3), and there is no power flow in branch 1-2 as shown in Figure 6b. As observed from the branch power flow for S2-R1 & S3-R1, there is a small amount of power exchange among the MGs because, for a weekly run R1, 1) the PV generation and battery in each MG are able to support its own load, and 2) the optimization strategy tries to reduce the unnecessary power loss in the branches.

Since MG1 has larger rated PV power, MG2 & MG3 have larger rated battery storage, and the total demand of MG2 is larger than that of MG3 as shown in Table 1, for the daily run S2-R2 under normal connected operating conditions, MG1 tends to send extra solar power to the other two MGs, and MG3 tends to send extra power to MG2 as indicated by its branch power flow in Figure 6a. Similarly, for the daily power flow run S3-R2 in Figure 6b, power flows from MG1 to MG3 and then from MG3 to MG2 for some portions of day 1 and day 3 since branch 1-2 is defective.

Under connected operating conditions, the batteries SOC could vary at the end of each day according to the power sharing among the MGs, therefore the fairness constraint F1 is employed to have a fairer power sharing among the MGs and be better prepared for contingencies that may lead to isolated MGs. The case S3-R2-F1 in Figure 4b shows the SOC with the fairness constraint that requires SOC gaps among MGs should not exceed 5% at any time, meantime, the branch power flows of S2-R2-F1 & S3-R2-F1 in Figure 6 have supported that power sharing is more frequent with

TABLE 2. Summary of results for the 3-MG system in puerto rico.

Case combination	Total load shedding (kVA)	Total PV generation (kVA)		PV curtailment (kVA)			Total charging-discharging (kVA)		
		MG1	MG2 = MG3	MG1	MG2	MG3	MG1	MG2	MG3
S1-R1	0	14710.10	11324.63	5570.50	253.15	1711.83	600.90	851.26	1037.80
S1-R2	0	14710.10	11324.63	5570.50	253.15	1711.83	600.90	851.26	1037.80
S1-R2-C1	608.78 (MG1)	7355.05	11324.63	0	253.15	1711.83	-492.62	851.26	1037.80
S1-R2-C2	608.78 (MG1)	7355.05	9625.94	0	0	50.53	-492.62	-536.36	992.77
S2-R1	0	14710.10	11324.63	5553.43	268.71	1698.76	600.89	867.27	1037.79
S2-R2	0	14710.10	11324.63	4730.94	760.96	2033.61	600.90	867.27	1037.80
S2-R2-F1	0	14710.10	11324.63	5040.75	905.96	1579.32	600.91	886.47	1018.59
S2-R2-C1	0	7355.05	11324.63	0	4.78	322.54	420.33	856.00	1037.80
S2-R2-C2	0	7355.05	9625.94	0	0	0	-490.55	-680.31	543.86
S3-R1	0	14710.10	11324.63	5563.73	259.57	1700.82	600.89	863.51	1037.79
S3-R2	0	14710.10	11324.63	5034.33	467.55	2026.49	600.90	863.50	1037.79
S3-R2-F1	0	14710.10	11324.63	5437.93	795.42	1297.33	609.24	880.65	1012.76
S3-R2-C1	0	7355.05	11324.63	0	441.65	267.77	58.23	855.98	1037.80
S3-R2-C2	0	7355.05	9625.94	0	0	0	-490.57	-524.21	387.90

the fairness constraint as compared to the cases without the fairness constraint.

By considering the contingency cases, the largest PV power generation (in MG1) is reduced to half in C1 & C2 settings. With the connected scenarios S2-R2-C2 & S3-R2-C2, MG3 mostly provided the extra power to MG1 as indicated by the power flows in Figure 6, and as compared to the independent case S1-R2-C2, the overall charged amount of MG3 battery is dropped from 992.77 kW to 387.90 kW in Table 2.

In summary, the connected MGs scenarios avoided load shedding with all combined settings and improved the power supply reliability under two contingency settings. All the numerical results presented in this section have further illustrated the effectiveness of the proposed restoration strategy using a real-world case study.

B. HIL TESTING AND RESULTS

After presenting the results for the Puerto Rico 3-MG system, in this section, the validation of such simulated results is conducted at one of the Oak Ridge National Laboratory HIL testbeds [55]. To implement the hardware testing, the 3-MG system is represented by the schematic in Figure 7.

Each microgrid consists of PV inverter, ESS (both modeled as a two level three phase inverter with inductive and capacitive LCL filter), point of common coupling (PCC) switch, dynamic PQ loads, and inductive-resistive (LR) line sections. The PCC switch incorporates synch check capabilities to ensure the voltage, frequency, and phase of the microgrids are aligned before closing the breaker. The real-time HIL simulator uses the profiles in Figure 2c for the aggregated load of the businesses and the solar irradiance obtained from the installed sensors in the 3-MG system.

Figure 8 shows the HIL setup used to conduct the experiments. The HIL testbed is composed of two paralleled Typhoon HIL 604 and one SEL 651R advanced recloser control. The SEL 651R are in the loop with the real time simulator to approximate the setup to the real system implementation. The Typhoon 604 is connected to the SEL

devices through a Typhoon HIL Connect, which provides analog and digital signals to the SEL-651R relays. These signals represent the analog voltage and current inputs to the relays, the binary outputs for opening and closing each SEL 651R recloser, and a binary status input to the relay to indicate the state of the breaker (open/close). The developed optimization model runs on a separate personal computer (PC), establishing communications with the real-time simulator through Modbus. The open-source Python package pyModbusTCP was implemented to establish the Modbus master on the PC. The real-time simulator uses a proprietary Modbus server to send and receive data from an external source.

To compare the results obtained from simulation and HIL testing, the SOCs of the batteries are selected for comparison, as they reflect the system dynamics. Figure 9 displays and compares the batteries SOCs of the three MGs under different case scenarios. The dark solid lines represent the optimization simulation results, while the light solid lines represent the HIL results. It can be observed that the batteries SOCs from the simulated and HIL testing results match closely in all cases. Note that since the other HIL results firmly match the simulated ones presented in Section III-A, we did not present all HIL results herein, as they will be similar and redundant to the simulated ones.

IV. CASE STUDY USING THE MODIFIED IEEE 33-BUS TEST DISTRIBUTION SYSTEM

In Section III, we have demonstrated the effectiveness of the proposed restoration strategy on a small 3-MG system, which may represent a weak grid condition. In this section, the modified IEEE 33-bus test distribution system that represents a good grid condition is considered to further illustrate and validate the proposed restoration strategy on a larger network system.

A. MODEL PARAMETERS AND EXPERIMENTAL SETTING

The employed IEEE 33-bus system is shown in Figure 10a. Unlike the real-world system considered in Section III, in this

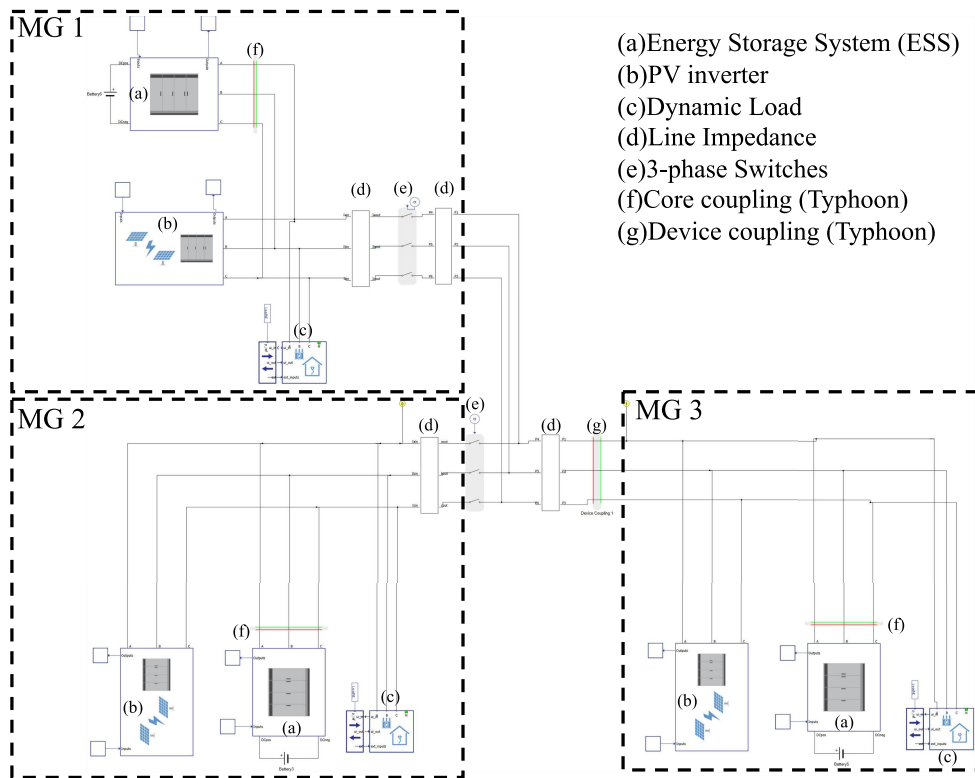


FIGURE 7. Typhoon HIL schematic for the Adjuntas 3-MG system. Each MG consists of PV generation, ESS, and load.



FIGURE 8. The implemented HIL testbed, which consists of (a) Typhoon Power Amplifier, (b,c) two Typhoon HIL 604 working in parallel, (d) Netgear network switches, (e) DER protocol translators, (f) SEL 651 R, and (g) SEL 3355 industrial computer.

modified bus system, the distance between each bus can be large. And each bus may represent an independent MG,

hence, to make it more general, we assume that each bus has MT, PV generation, and battery ESS. However, the power ratings for such DERs can be assigned to zero. Each bus serves either a critical load or an interruptible (noncritical) load. Solid black lines indicate the branches without remotely controlled switches (RCS), while green colored branches have RCS. Dashed lines are normally open and can be closed if needed. The energy systems capacities and the power load of each bus are stacked in the bar chart in Figure 10b. For the DER capacity settings, the MTs maximum generation power at each bus is set in the range $(0.6 \sim 0.9) \cdot \bar{S}$, where \bar{S} is the maximum apparent load power at the corresponding bus, PV maximum generation power is set to be $2 \cdot \bar{S}$, and battery maximum power capacity is set to be $3 \cdot \bar{S}$. The upper limit of ramping up \bar{U} and ramping down \bar{D} for a MT is set to be 5% of the MT generation upper limit \bar{G} in Figure 10b.

The hourly solar irradiance and basis load shapes are shown in Figure 11. The solar PV power generation is computed by multiplying the rated power of the PV system in Figure 10b and the solar irradiance in Figure 11 for each hour. Similarly, the hourly real/reactive load demand of each bus equals the corresponding real/reactive power load in Figure 10b times the basis load in Figure 11 for critical and interruptible load buses. The operation cost of MT is $C^G = 0.25\$/kW$, and the other model parameters are the same as the ones in Section III-A. One day operation is considered for this case study, and the thermal limit of each line has been

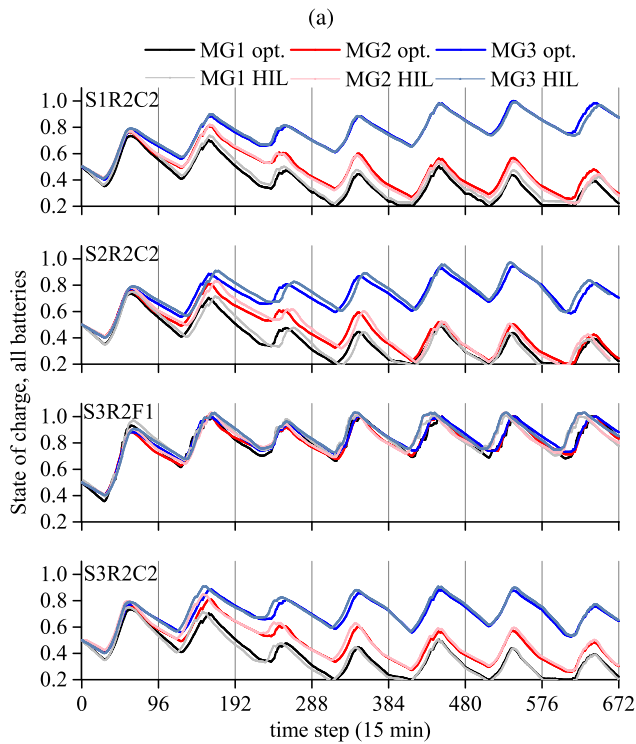
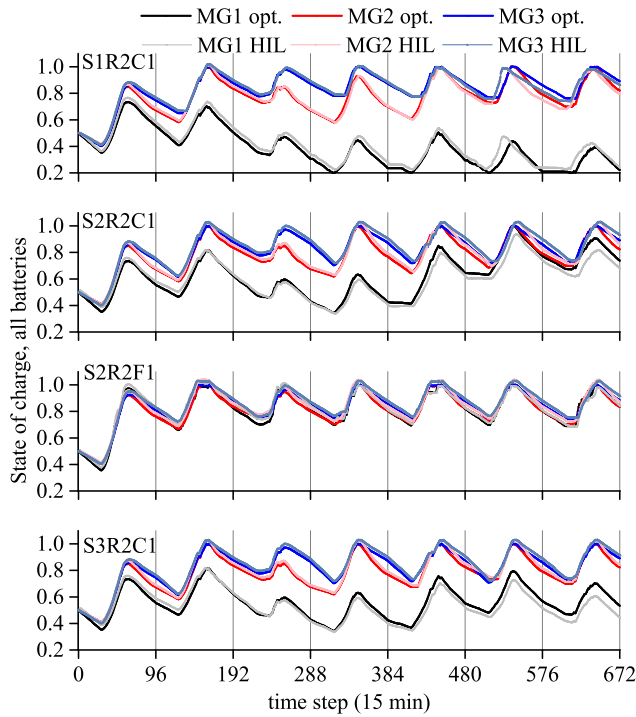
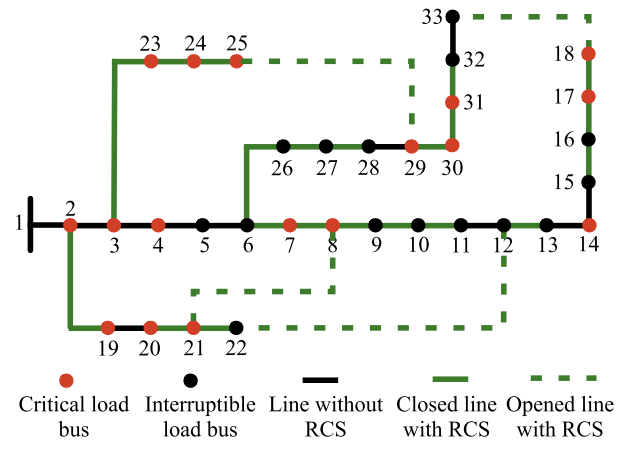
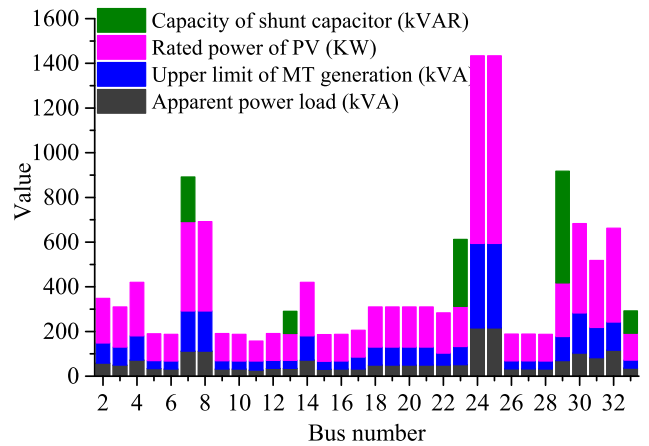


FIGURE 9. Battery SOC comparison between HIL testing and numerical optimization results for the 3-MG system in Puerto Rico under different settings.

set large enough to better demonstrate the network restoration solutions. Otherwise, the feasibility of the restoration solution will be limited.



(a) MT, PV, and ESS are assumed at each bus.



(b) Load and generation settings at each bus.

FIGURE 10. The modified IEEE 33-bus test distribution system and its load-generation settings.

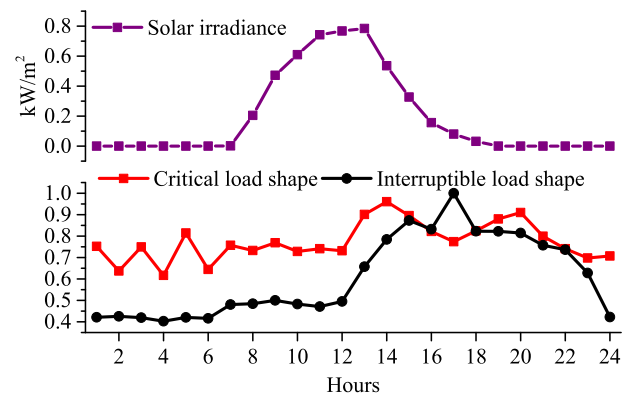
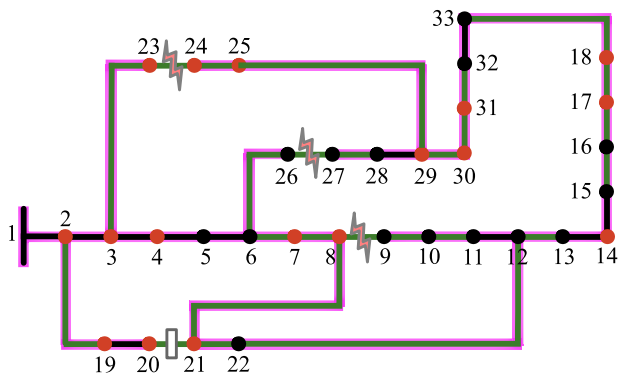


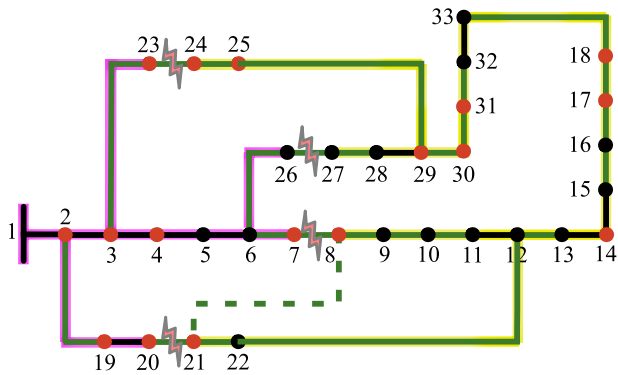
FIGURE 11. Load shapes and solar irradiance at all buses.

B. RECONFIGURATION WITH LINE FAULTS

In this case study, bus 1 is assumed to be disconnected from the main distribution grid, so only the islanded mode is considered here. Two representative scenarios are considered: 1) 3 line outages in line 8-9, line 23-24, line 26-27, and 2) 4 line outages in line 7-8, line 20-21, line 23-24,



(a) Optimized topology with 3 line outages.



(b) Optimized topology with 4 line outages.

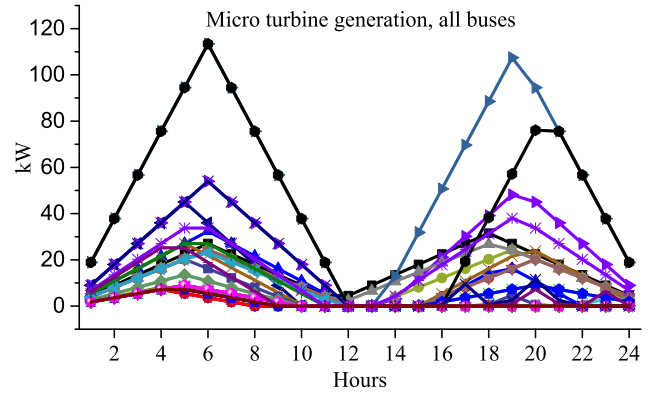
FIGURE 12. Network reconfiguration cases with different line outages.

TABLE 3. Summary of results for the IEEE 33-bus system.

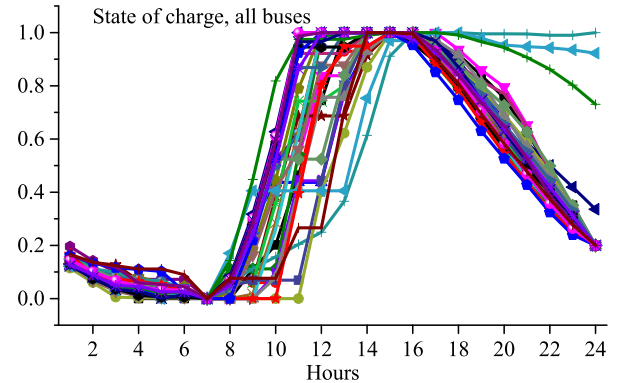
Value	3-line outage	4-line outage
Objective value (\$)	7314.52	8706.82
MT generation (kVA)	7293.12	7036.72
Total solar generation (kW)	35023.71	35023.71
Consumed solar generation (kW)	23584.30	22842.67
Battery degradation cost (\$)	173.86	171.39
Total battery charging (kVA)	11172.05	11185.28
Total battery discharging (kVA)	10560.48	10239.11
Critical load shedding (kVA)	1241.51	1475.85
Interruptible load shedding (kVA)	2093.33	3176.23

line 26-27. The reconfigured network topology for the two considered scenarios are shown in Figures 12a and 12b. As shown in Figure 12a, with the 3 line outages, the optimal reconfiguration is to open line 20-21 and close all other opened lines with RCS. With the 4 line outages in Figure 12b, the 33-bus system is actually divided into two separate subsystems. The optimal result is to open the switch in line 8-21 to avoid cycles and maintain the radial topology structure indicated by Eqs.(2)-(6).

Take the 3 line outage scenario for instance, the MT generation settings and the SOC profiles for batteries are illustrated in Figure 13. Since the solar PV power has a peak at around noon (hour 12), the MT generation of all buses has formatted double peak shape in the early morning



(a) MT generation.



(b) Battery state of charge.

FIGURE 13. Energy scheduling of MTs and batteries for the 3 line outage scenario (each curve represents a bus).

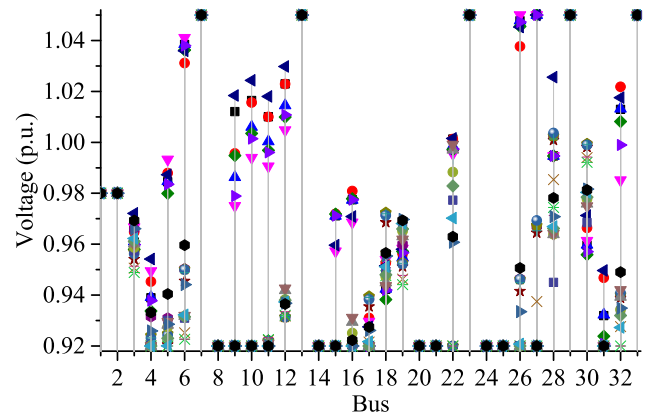


FIGURE 14. Voltages for all buses in 24 hours (there are 24 values on each vertical line, each value represents one hour of simulation time).

(hours 5-6) and late afternoon (hours 19-20) with a valley at around noon time. A similar trend is observed for the batteries SOC that follows the solar irradiance shape; all batteries discharge in the early morning (before hour 8) and late afternoon (after hour 16) to support load power demand, and they start charging when the solar irradiance starts to rise up around hour 8 until their SOC reaches the maximum level around solar peak hour.

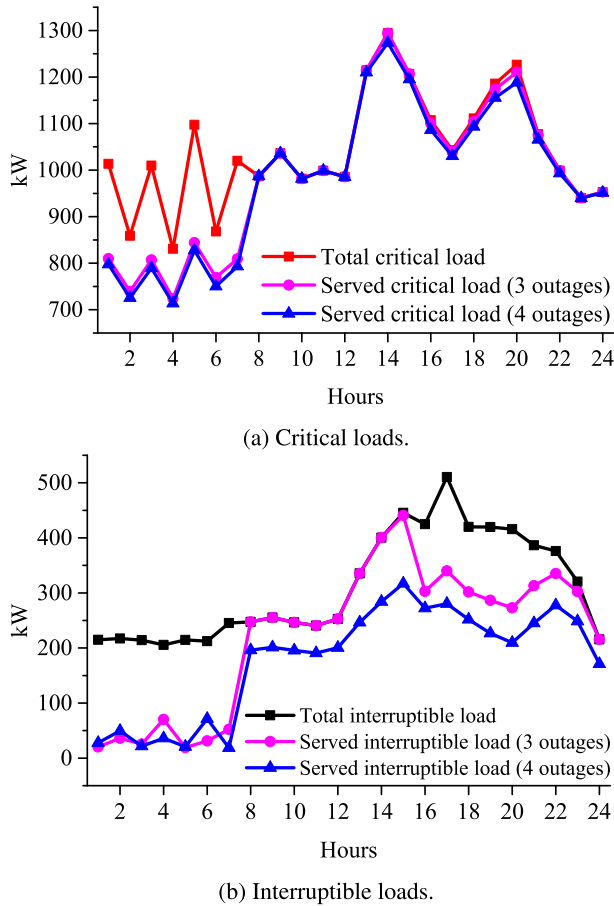


FIGURE 15. Served loads for the 3 and 4 line outage scenarios.

Figure 14 shows the per unit voltages for all buses for the 3 line outage scenario. It is observed that the bus voltages were maintained within the permissible limits (0.92 - 1.05) at all times as set by the hard constraint in Eq.(24). The voltage at buses 7, 13, 23, 29, 33 is at highest level because shunt capacitors are located at these buses, as indicated by the green bars in Figure 10b.

The served load profiles of the IEEE 33-bus system are presented in Figure 15 for the two outage scenarios. While the served critical and interruptible loads were both reduced when line outages number increased, the shed interruptible load was much larger due to its lower cost. For 24-hour optimization, the detailed results are summarized in Table 3. By comparing the results of the 3 line and 4 line outages in Table 3, it can be observed that if there are more open paths as in the case of the 4 line outage, this will make the network less robust, and the power absorption will decrease, and its reliability will decrease. For instance, as previously illustrated, the 33-bus system was completely divided into two disconnected subsystems in the 4 line outage scenario. Even reconfiguring the network could not bridge the two separated subsystems, the MT generation and battery discharging have been reduced as compared to the 3 line

outage scenario, as they could not provide the needed power to the other subsystem, leading to higher load shedding.

V. CONCLUSION

Aiming at resilience improvement for power delivery during extreme events, a comprehensive network topology reconfiguration and DERs scheduling optimization strategy for distribution grids was formulated in this research. The proposed optimization strategy is linear, so it does not require heavy computations and can thus be easily implemented in real-time. The proposed strategy is then tested on the modified IEEE 33-bus system and the 3-MG system in Adjuntas public plaza, Puerto Rico using real PV generation, load demand, and weather data collected from the field.

The experimental results have demonstrated the benefits in resilience improvement and cost saving from the topology reconfiguration and network power sharing strategies under various conditions. For example, in the Adjuntas community 3-MG networked system case study, a load shedding with an amount of 608.78 kVA in the independent scenario has been avoided using the connected MGs scenario under the considered two contingency settings. Thus, the network of MGs can significantly enhance the islanded operation during contingencies by sharing resources such as PV generation and ESS, where local critical loads of the affected MG can be supported by external generation, thus reducing load shedding or extending sustained periods.

In summary, a few key takeaways from this research are:

- System restoration using network topology reconfiguration together with optimal scheduling of DERs leads to more resilient distribution systems (i.e., reduced or zero load shedding).
- Networked MGs could overcome the problem of unevenly distributed generation and demand among individual MGs during normal operation and minimize critical load shedding in extreme scenarios.
- The unfairness of battery operation exists in networked MGs (i.e., some batteries discharge excessively while others operate in a more conservative way). Thus, fairness constraints should be considered in practical settings.

Nowadays, we are preparing to field test and validate the proposed restoration strategy in the networked 3-MG system in Adjuntas, Puerto Rico. This will field demonstrate the applicability of the proposed strategy and its model's assumptions in a real-world testing environment. We expect to start the field testing in the next few months. Furthermore, since the proposed network reconfiguration and DERs scheduling restoration strategy for distribution systems and networked MGs is deterministic, future work is to investigate a *stochastic* version of it to account for the inherent uncertainties in the system such as PV power generation, load power consumption, and faults' locations.

ACKNOWLEDGMENT

This manuscript has been authored by UT-Battelle, LLC, under contract DE-AC05-00OR22725 with the US Department of Energy (DOE). The US government retains and the publisher, by accepting the article for publication, acknowledges that the US government retains a nonexclusive, paid-up, irrevocable, worldwide license to publish or reproduce the published form of this manuscript, or allow others to do so, for US government purposes. DOE will provide public access to these results of federally sponsored research in accordance with the DOE Public Access Plan (<http://energy.gov/downloads/doe-public-access-plan>).

REFERENCES

- [1] U.S. Energy Inf. Admin. (2022). *Average Duration of Total Annual Electric Power Interruptions*. Accessed: Nov. 21, 2024. [Online]. Available: <https://www.eia.gov/todayinenergy/detail.php?id=12345>
- [2] Climate Central. (2022). *Surging Weather-related Power Outages*. Accessed: Nov. 21, 2024. [Online]. Available: <https://www.climatecentral.org/climate-matters/surging-weather-related-power-outages>
- [3] A. Umunnakwe, M. Parvania, H. Nguyen, J. D. Horel, and K. R. Davis, "Data-driven spatio-temporal analysis of wildfire risk to power systems operation," *IET Gener., Transmiss. Distrib.*, vol. 16, no. 13, pp. 2531–2546, Jul. 2022.
- [4] A. Nejat, L. Solitare, E. Pettitt, and H. Mohsenian-Rad, "Equitable community resilience: The case of winter storm uri in Texas," *Int. J. Disaster Risk Reduction*, vol. 77, Jul. 2022, Art. no. 103070.
- [5] T. Kemabonta, "Grid resilience analysis and planning of electric power systems: The case of the 2021 Texas electricity crises caused by winter storm uri (#TexasFreeze)," *Electr. J.*, vol. 34, no. 10, Dec. 2021, Art. no. 107044.
- [6] FiscalNotes. (2022). *Winter Storm Uri 2021—The Economic Impact of the Storm*. Accessed: Nov. 21, 2024. [Online]. Available: <https://comptroller.texas.gov/economy/fiscal-notes/2021/oct/winter-storm-impact.php>
- [7] Univ. Texas at Austin. (2022). *The Timeline and Events of the February 2021 Texas Electric Grid Blackouts*. Accessed: Nov. 21, 2024. [Online]. Available: [https://www.puc.texas.gov/agency/resources/reports/utaustin_\(2021\)_eventsfebruary2021texasblackout_\(002\)final_07_12_21.pdf](https://www.puc.texas.gov/agency/resources/reports/utaustin_(2021)_eventsfebruary2021texasblackout_(002)final_07_12_21.pdf)
- [8] M. O. Román, E. C. Stokes, R. Shrestha, Z. Wang, L. A. Schultz, E. A. S. Carlo, Q. Sun, J. R. Bell, A. Molthan, V. Kalb, C. Ji, K. C. Seto, S. N. McClain, and M. Enenkel, "Satellite-based assessment of electricity restoration efforts in Puerto Rico after Hurricane Maria," *PLoS ONE*, vol. 14, no. 6, Jun. 2019, Art. no. e0218883.
- [9] Federal Emergency Manage. Agency. (2022). *Puerto Rico Hurricane Fiona: DR-4671-PR*. Accessed: Nov. 21, 2024. [Online]. Available: <https://www.fema.gov/disaster/4671>
- [10] M. N. Albasrawi, N. Jarus, K. A. Joshi, and S. S. Sarvestani, "Analysis of reliability and resilience for smart grids," in *Proc. IEEE 38th Annu. Comput. Softw. Appl. Conf.*, Jul. 2014, pp. 529–534.
- [11] D. K. Mishra, M. J. Ghadi, A. Azizvahed, L. Li, and J. Zhang, "A review on resilience studies in active distribution systems," *Renew. Sustain. Energy Rev.*, vol. 135, Jan. 2021, Art. no. 110201.
- [12] F. H. Jufri, V. Widiputra, and J. Jung, "State-of-the-art review on power grid resilience to extreme weather events: Definitions, frameworks, quantitative assessment methodologies, and enhancement strategies," *Appl. Energy*, vol. 239, pp. 1049–1065, Apr. 2019.
- [13] R. B. Duffey and T. Ha, "The probability and timing of power system restoration," *IEEE Trans. Power Syst.*, vol. 28, no. 1, pp. 3–9, Feb. 2013.
- [14] R. Nateghi, S. D. Guikema, and S. M. Quiring, "Forecasting hurricane-induced power outage durations," *Natural Hazards*, vol. 74, no. 3, pp. 1795–1811, Dec. 2014.
- [15] T. Walsh, T. Layton, D. Wanik, and J. Mellor, "Agent based model to estimate time to restoration of storm-induced power outages," *Infrastructures*, vol. 3, no. 3, p. 33, Aug. 2018.
- [16] A. Arif, S. Ma, Z. Wang, J. Wang, S. M. Ryan, and C. Chen, "Optimizing service restoration in distribution systems with uncertain repair time and demand," *IEEE Trans. Power Syst.*, vol. 33, no. 6, pp. 6828–6838, Nov. 2018.
- [17] N. Safaei, D. Banjevic, and A. K. S. Jardine, "Workforce planning for power restoration: An integrated simulation-optimization approach," *IEEE Trans. Power Syst.*, vol. 27, no. 1, pp. 442–449, Feb. 2012.
- [18] Executive Office President. (2013). *Economic Benefits of Increasing Electric Grid Resilience To Weather Outages*. Accessed: Nov. 21, 2024. [Online]. Available: https://www.energy.gov/sites/prod/files/2013/08/f2/Grid%20Resiliency%20Report_FINAL.pdf
- [19] A. Arab, E. Tekin, A. Khodaei, S. K. Khator, and Z. Han, "System hardening and condition-based maintenance for electric power infrastructure under Hurricane effects," *IEEE Trans. Rel.*, vol. 65, no. 3, pp. 1457–1470, Sep. 2016.
- [20] W. Hughes, W. Zhang, A. C. Bagtzoglou, D. Wanik, O. Pensado, H. Yuan, and J. Zhang, "Damage modeling framework for resilience hardening strategy for overhead power distribution systems," *Rel. Eng. Syst. Saf.*, vol. 207, Mar. 2021, Art. no. 107367.
- [21] Y. Lin and Z. Bie, "Tri-level optimal hardening plan for a resilient distribution system considering reconfiguration and DG islanding," *Appl. Energy*, vol. 210, pp. 1266–1279, Jan. 2018.
- [22] N. L. Dehghani, A. B. Jeddi, and A. Shafieezadeh, "Intelligent Hurricane resilience enhancement of power distribution systems via deep reinforcement learning," *Appl. Energy*, vol. 285, Mar. 2021, Art. no. 116355.
- [23] D. Anokhin, P. Dehghanian, M. A. Lejeune, and J. Su, "Mobility-as-a-service for resilience delivery in power distribution systems," *Prod. Oper. Manage.*, vol. 30, no. 8, pp. 2492–2521, Aug. 2021.
- [24] B. Taheri, A. Safdarian, M. Moeini-Aghtaie, and M. Lehtonen, "Distribution system resilience enhancement via mobile emergency generators," *IEEE Trans. Power Del.*, vol. 36, no. 4, pp. 2308–2319, Aug. 2021.
- [25] J. Kim and Y. Dvorkin, "Enhancing distribution system resilience with mobile energy storage and microgrids," *IEEE Trans. Smart Grid*, vol. 10, no. 5, pp. 4996–5006, Sep. 2019.
- [26] A. K. Erenoglu, S. Sancar, I. S. Terzi, O. Erdinc, M. Shafie-Khah, and J. P. S. Catalão, "Resiliency-driven multi-step critical load restoration strategy integrating on-call electric vehicle fleet management services," *IEEE Trans. Smart Grid*, vol. 13, no. 4, pp. 3118–3132, Jul. 2022.
- [27] F. Hafiz, B. Chen, C. Chen, A. Rodrigo de Queiroz, and I. Husain, "Utilising demand response for distribution service restoration to achieve grid resiliency against natural disasters," *IET Gener., Transmiss. Distribution*, vol. 13, no. 14, pp. 2942–2950, Jul. 2019.
- [28] Y. Chen and M. Hu, "Balancing collective and individual interests in transactive energy management of interconnected micro-grid clusters," *Energy*, vol. 109, pp. 1075–1085, Aug. 2016.
- [29] Y. Chen, B. Park, X. Kou, M. Hu, J. Dong, F. Li, K. Amasyali, and M. Olama, "A comparison study on trading behavior and profit distribution in local energy transaction games," *Appl. Energy*, vol. 280, Dec. 2020, Art. no. 115941.
- [30] K. Amasyali, Y. Chen, B. Telsang, M. Olama, and S. M. Djouadi, "Hierarchical model-free transactional control of building loads to support grid services," *IEEE Access*, vol. 8, pp. 219367–219377, 2020.
- [31] K. Amasyali, Y. Chen, and M. Olama, "A data-driven, distributed game-theoretic transactional control approach for hierarchical demand response," *IEEE Access*, vol. 10, pp. 72279–72289, 2022.
- [32] X. Liang, M. A. Saaklayen, M. A. Igder, S. M. R. H. Shawon, S. O. Faried, and M. Janbakhsh, "Planning and service restoration through microgrid formation and soft open points for distribution network modernization: A review," *IEEE Trans. Ind. Appl.*, vol. 58, no. 2, pp. 1843–1857, Mar. 2022.
- [33] Q. Shi, F. Li, M. Olama, J. Dong, Y. Xue, M. Starke, W. Feng, C. Winstead, and T. Kuruganti, "Post-extreme-event restoration using linear topological constraints and DER scheduling to enhance distribution system resilience," *Int. J. Electr. Power Energy Syst.*, vol. 131, Oct. 2021, Art. no. 107029.
- [34] Q. Shi, F. Li, M. Olama, J. Dong, Y. Xue, M. Starke, C. Winstead, and T. Kuruganti, "Network reconfiguration and distributed energy resource scheduling for improved distribution system resilience," *Int. J. Electr. Power Energy Syst.*, vol. 124, Jan. 2021, Art. no. 106355.
- [35] M. Zare-Bahramabadi, A. Abbaspour, M. Fotuhi-Firuzabad, and M. Moeini-Aghtaie, "Resilience-based framework for switch placement problem in power distribution systems," *IET Gener., Transmiss. Distribution*, vol. 12, no. 5, pp. 1223–1230, Mar. 2018.
- [36] C. Chen, J. Wang, F. Qiu, and D. Zhao, "Resilient distribution system by microgrids formation after natural disasters," *IEEE Trans. Smart Grid*, vol. 7, no. 2, pp. 958–966, Mar. 2016.

- [37] Y.-J. Kim, J. Wang, and X. Lu, "A framework for load service restoration using dynamic change in boundaries of advanced microgrids with synchronous-machine DGs," *IEEE Trans. Smart Grid*, vol. 9, no. 4, pp. 3676–3690, Jul. 2018.
- [38] J. Zhao, F. Li, S. Mukherjee, and C. Sticht, "Deep reinforcement learning-based model-free on-line dynamic multi-microgrid formation to enhance resilience," *IEEE Trans. Smart Grid*, vol. 13, no. 4, pp. 2557–2567, Jul. 2022.
- [39] Edison Electric Inst. (2014). *Before And After The Storm: A Compilation of Recent Studies, Programs, and Policies Related To Storm Hardening and Resiliency*. Accessed: Nov. 21, 2024. [Online]. Available: <https://pdii.org/wp-content/uploads/2021/03/245-BeforeandAftertheStorm.pdf>
- [40] W. Wang, X. Xiong, Y. He, J. Hu, and H. Chen, "Scheduling of separable mobile energy storage systems with mobile generators and fuel tankers to boost distribution system resilience," *IEEE Trans. Smart Grid*, vol. 13, no. 1, pp. 443–457, Jan. 2022.
- [41] S. Jafarpour and M. H. Amirioun, "A resilience-motivated restoration scheme for integrated electricity and natural gas distribution systems using adaptable microgrid formation," *IET Gener., Transmiss. Distribution*, vol. 17, no. 23, pp. 5223–5239, Dec. 2023.
- [42] I. M. Diahovchenko, G. Kandaperumal, and A. K. Srivastava, "Enabling resiliency using microgrids with dynamic boundaries," *Electric Power Syst. Res.*, vol. 221, Aug. 2023, Art. no. 109460.
- [43] A. D. Bintoudi and C. Demoulias, "Optimal isolated microgrid topology design for resilient applications," *Appl. Energy*, vol. 338, May 2023, Art. no. 120909.
- [44] Joint Capability Technol. Demonstration. (2015). *Smart Power Infrastructure Demonstration for Energy Reliability and Security (SPIDERS)*. Accessed: Nov. 21, 2024. [Online]. Available: https://www.energy.gov/sites/prod/files/2016/03/f30/spiders_final_report.pdf
- [45] Bonneville Power Authority. (2022). *Power Grid Gets Smarter With New Oregon MG*. Accessed: Nov. 21, 2024. [Online]. Available: <https://www.bpa.gov/energy-and-services/efficiency/smart-grid/pacific-northwest-demo-project>
- [46] C. Marnay, N. DeForest, and J. Lai, "A green prison: The Santa Rita jail campus microgrid," in *Proc. IEEE Power Energy Soc. Gen. Meeting*, Jul. 2012, pp. 1–2.
- [47] U.S. Dept. Energy, Electr. Del. & Energy Rel. (2015). *2015 Progress Report for OE ARRA Smart Grid Demonstration Program: Aggregation of RDSI, SGDP, and SGIG Results*. Accessed: Nov. 21, 2024. [Online]. Available: https://www.energy.gov/sites/prod/files/2016/12/f34/Activity%206%20Report_Public_Version_051415%20FINAL.pdf
- [48] H. Katmale, S. Clark, T. Bialek, L. Abcede. (2019). *California Energy Commission, Borrego Springs: California's First Renewable Energy-Based Community Microgrid*. California Energy Commission. Accessed: Nov. 21, 2024. [Online]. Available: <https://www.energy.ca.gov/sites/default/files/2021-05/CEC-500-2019-013.pdf>
- [49] D. T. Ton and M. A. Smith, "The U.S. department of energy's microgrid initiative," *Electr. J.*, vol. 25, no. 8, pp. 84–94, Oct. 2012.
- [50] H. Farzin, M. Fotuhi-Firuzabad, and M. Moeini-Aghtaie, "Role of outage management strategy in reliability performance of multi-microgrid distribution systems," *IEEE Trans. Power Syst.*, vol. 33, no. 3, pp. 2359–2369, May 2018.
- [51] M. Daneshvar, B. Mohammadi-Ivatloo, K. Zare, S. Asadi, and A. Anvari-Moghaddam, "A novel operational model for interconnected microgrids participation in transactive energy market: A hybrid IGDT/stochastic approach," *IEEE Trans. Ind. Informat.*, vol. 17, no. 6, pp. 4025–4035, Jun. 2021.
- [52] P. H. Kumar and R. Mageshvaran, "Methods and solvers used for solving mixed integer linear programming and mixed nonlinear programming problems: A review," *Int. J. Sci. Technol. Res.*, vol. 9, no. 1, pp. 1872–1882, Jan. 2020.
- [53] (2024). *Gurobi Optimization*. Accessed: Nov. 21, 2024. [Online]. Available: <https://www.gurobi.com/>
- [54] Oak Ridge Nat. Lab. (2022). *Researchers Bring More Reliable Electricity to Puerto Rican Microgrids*. Accessed: Nov. 21, 2024. [Online]. Available: <https://www.ornl.gov/news/researchers-bring-more-reliable-electricity-puerto-rican-microgrids>
- [55] Oak Ridge Nat. Lab. (2022). *Advancing Grid Resiliency, Security With a Microgrid Test Bed: SI-GRID*. Accessed: Nov. 21, 2024. [Online]. Available: <https://www.ornl.gov/research-highlight/advancing-grid-resiliency-security-microgrid-test-bed-si-grid>



YANG CHEN (Member, IEEE) received the B.S. degree from Henan Polytechnic University, Henan, China, in 2010, the M.S. degree from Chongqing University, Chongqing, China, in 2013, and the Ph.D. degree in industrial engineering and operation research from the University of Illinois at Chicago, IL, USA, in 2018. He is currently a Research Scientist with the Computational Sciences and Engineering Division, Oak Ridge National Laboratory. His research interests

include energy system operation in smart buildings, developing efficient coordinating algorithms for building level microgrids to exchange and trade energy in emerging local energy transaction market. He is particularly interested and has a great passion in renewable energy technologies and smart grid optimization. His other research interests include power system restoration and learning based decision making.



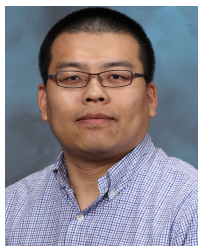
MOHAMMED OLAMA (Senior Member, IEEE) received the B.S. and M.S. (Hons.) degrees in electrical engineering from the University of Jordan, Amman, Jordan, in 1998 and 2001, respectively, and the Ph.D. degree from the Electrical Engineering and Computer Science (EECS) Department, University of Tennessee, Knoxville, TN, USA, in 2007. He is currently a Senior Research Scientist with the Computational Sciences and Engineering Division, Oak Ridge

National Laboratory (ORNL), Oak Ridge, TN, USA. He is also an Adjunct Associate Professor with the EECS Department, University of Tennessee, Knoxville. At ORNL, he has led and participated in several projects under various DOE, DOD, and DHS programs. He has been involved in various modeling, simulations, controls, and communications projects for improved critical infrastructure efficiency, reliability, and security including the smart grid and healthcare. He has more than 180 archival publications (including journals, conference proceedings, book chapters, and technical reports) in addition to numerous presentations at professional conferences and international symposia. His research interests include smart grid and smart buildings, smart grid communications and control, building-to-grid integration, renewable energy integration, wide-area monitoring and control, microgrid operation and control, cyber-physical systems, complex systems, wireless communications, data analytics, statistical signal processing, and machine learning.



MAXIMILIANO F. FERRARI (Senior Member, IEEE) received the B.S. degree in electrical engineering from the University of Javeriana, the B.S. degree in physics from Allegheny College, the M.S. degree in electrical engineering from the Polytechnic University of Valencia, and the Ph.D. degree in energy sciences from the University of Tennessee, Knoxville. He is currently a Research and Development Staff Member with the Grid Components and Controls Group, Oak Ridge

National Laboratory. His research interests include microgrids, controls of solar and wind energy systems, and protection.



GUODONG LIU (Senior Member, IEEE) received the Ph.D. degree in electrical engineering from the University of Tennessee, Knoxville, TN, USA, in 2014. Since 2014, he has been a Research and Development Staff with the Electrical and Electronic System Research Division, Oak Ridge National Laboratory (ORNL), where he currently leads projects on microgrid operation and planning, renewable energy integration, and active distribution network management. He is the major

developer of CSEISMIC microgrid controller, Si-grid, DECC microgrid, and RTDS-based microgrid testbed. He is the Principal Investigator of MADRA sponsored by the DOE Office of Electricity Delivery and Energy (DOE-OE). His research interests include power system operation and planning, power system reliability and security assessment, distributed energy resources, and microgrids.



BYUNGKWON PARK (Member, IEEE) received the B.S. degree in electrical engineering from Chonbuk National University, South Korea, in 2011, and the M.S. and Ph.D. degrees in electrical engineering from the University of Wisconsin–Madison, Madison, WI, USA, in 2014 and 2018, respectively. He is currently an Assistant Professor with the Department of Electrical Engineering, Soongsil University (SSU), Seoul, South Korea. Before joining SSU,

he was a Research Staff with the Computational Sciences and Engineering Division, Oak Ridge National Laboratory. His research interests include modeling, simulation, control, and optimization of electrical energy systems.



QINGXIN SHI (Member, IEEE) received the B.S. degree from Zhejiang University, China, in 2011, the M.Sc. degree from the University of Alberta, Canada, in 2014, and the Ph.D. degree from the University of Tennessee, Knoxville, USA, in 2019. He was a Research Assistant Professor with the University of Tennessee, Knoxville, from 2019 to 2020. He is currently an Assistant Professor with the School of Electrical and Electronic Engineering, North China Electric Power

University, Beijing, China. His research interests include demand response and resilient urban power systems.



ARTURO A. MASSOL-DEYA (Member, IEEE) received the Ph.D. degree from the Center for Microbial Ecology, Michigan State University, in 1994. Since then, he has been a Faculty Member with the Department of Biology, University of Puerto Rico at Mayagüez, Mayagüez Campus. He is currently the Executive Director of Casa Pueblo, Adjuntas, a community-based group in Puerto Rico with 40 years of services in natural resources conservation, education, and sustainable development.



ADITYA SUNDARARAJAN (Senior Member, IEEE) received the M.S. degree in computer engineering and the Ph.D. degree in electrical and computer engineering from Florida International University, Miami. He is currently a Research and Development Associate Staff with the Grid Systems Architecture Group, Oak Ridge National Laboratory. His research interests include applied machine learning, privacy-preserving data analytics, and emerging data strategies to address

challenges in microgrids and distribution grid intelligence. He also serves as the Secretary for the IEEE PELS/PES East Tennessee Joint Chapter.



THOMAS B. OLLIS (Senior Member, IEEE) received the B.S. and M.S. degrees in electrical engineering from the University of Tennessee, Knoxville. He was with Oak Ridge National Laboratory (ORNL), in 2013, as a Student, and joined ORNL, as a full-time Staff Member, in 2014. He was a Distribution System Operator in college and also in system planning for transmission and distribution systems at Duke Energy. He is currently a Research and Development Staff with

the Grid Components and Controls Group, ORNL. His research interests include microgrids, battery energy storage, distribution market design, and renewable generation integration and control.

...